Available online at www.eccomasproceedia.org
Eccomas Proceedia COMPDYN (2017) 4847-4856

ECCOMAS
Proceedia

COMPDYN 2017
6th ECCOMAS Thematic Conference on
Computational Methods in Structural Dynamics and Earthquake Engineering
M. Papadrakakis, M. Fragiadakis (eds.)
Rhodes Island, Greece, 15–17 June, 2017

# SIMULATIONS OF CONCRETE FRACTURE AT VARIOUS STRAIN RATES: PARAMETRIC STUDY

**Josef Květoň**[1] **and Jan Eliáš**[1]

[1]Brno University of Technology, Faculty of Civil Engineering
Veveří 331/95, 602 00 Brno, Czech Republic
e-mail: kveton.j@fce.vutbr.cz; elias.j@fce.vutbr.cz

**Keywords:** Discrete model, Concrete fracture, Dynamics, Inertia, Strain Rate

**Abstract.** *The contribution presents numerical simulations of a recently published experimental series on concrete specimens. The numerical model mimics the meso-structure of the concrete by representing material via system of interconnected rigid polyhedral particles. These particles correspond to mineral aggregates and surrounding matrix. The geometry of particles is based on Voronoi tessellation. The particles are rigid, but they may move and rotate. The displacement jump at their contacts gives rise interaction forces defined by the constitutive relation in a vectorial form. The constitutive equations are independent of the strain rate. Simulations are dynamical, the time dependent response is calculated using Newmark implicit scheme. Full inertia tensor of every particle is taken into account when assembling the mass matrix.*

*To demonstrate the ability of the model to capture the strain rate dependence of the experimental results, series of specimens loaded under various displacement rates are simulated. For quasi-static loading, the initial microcracks usually localize into one highly damaged zone where main crack appears. With increasing strain rate, the amount of energy accumulated in the specimen body is not consumed by one crack only and crack branching occurs. The peak loading force increases with increasing rate as well.*

*Both the strain rate dependence of the loading force and crack branching phenomena are captured by the presented numerical model. The obtained results are compared with the experimental response of the simulated specimens. Parametric study of the model is performed showing different effect of various parameters under different strain rates.*


Peer-review under responsibility of the organizing committee of COMPDYN 2017.
doi: 10.7712/120117.5766.17557

## 1 INTRODUCTION

In modern engineering, understanding of material behavior is an integral part of structural design. The response of a structure is usually calculated numerically using models verified with help of laboratory tests. The choice of mathematical model is important; the material internal length and its relation to structure dimensions should be taken into consideration. If the heterogeneity of the material is relatively fine compared to the structure dimensions, the material can be conveniently treated as homogeneous and described using continuous formulation. Continuous formulation involves partial differential equations that can be numerically solved with a help of the finite element method (FEM), that provides approximations of the exact solution with high accuracy. In continuous models, fracture is usually represented by so called smeared crack. Material remains continuous, but its stiffness is being reduced as cracking occurs. Such approach brings need for regularization [3, 2]. Several other approaches incorporating discontinuities into FEM models has been presented in literature [10].

This contribution presents fracture simulations of concrete specimens with heterogeneity comparable to specimen size. At this scale, it is convenient to use meso-scale approach with direct representation of mineral aggregates. Such meso-scale model can be advantageously based on the discrete formulation. Discrete approaches were established by representing material by simple lattices of 1D elasto-brittle elements. The heterogeneity can be included e.g. using random lattice structure or by projection of concrete meso structure on the lattice [15]. In the latter case, the element material properties are set according to which phase they belong to – aggregate, cement paste or contact of cement paste with aggregate, so called interfacial transition zone (ITZ).

Another variant of discrete approach represents material as a system of interconnected rigid particles that typically correspond to one mineral grain (particle) with surrounding matrix. The motivation for choosing this variant for present contribution is in highly reduced computational cost of the particle approach compared to previously mentioned lattice approach. The model developed according to [4] is used within this contribution.

It is well known, that the loading capacity and failure mode is dependent on the strain rate applied. In quasi static loading, initial micro-cracks in the material localize into one highly damaged zone, so called macro-crack. With increasing strain rate, the energy in material body is not consumed by one crack only and more cracks appear, eventually one crack branches. This behavior has been observed experimentally in [12]. The presented contribution studies the behavior of the discrete model for concrete loaded under various displacement rates. Time integration is performed in an implicit scheme, contrary to other papers that use dynamical discrete models in connection with explicit time integration scheme [8, 13].

## 2 NUMERICAL MODEL

### 2.1 Particle approach

The 3D system of discrete particles is built according to [6], which is just simplified version of [4]. Particle centers come from process of random placing points in the domain, keeping their distance larger than parameter $l_{\min}$. This internal length dictates the particle size and to large extend also the nonlinear behavior of the model. Voronoi tessellation is performed to get the geometry of particles. Each particle is considered as ideally rigid, material model is applied at its contacts with other particles.

On the contacts (facets), normal and shear stiffness of particle connection is prescribed.

Relation between stress and strain on each facet yields

$$\sigma_i = (1-\omega)E_i\varepsilon_i \quad \text{for} \quad i = N, M, L \tag{1}$$

where $N$ is normal and $M$ and $L$ are two shear directions. The elastic behavior is described by the elastic modulus $E_0$ and normal-tangential stiffness ratio $\alpha$.

$$E_N = E_0, \quad E_{M,L} = \alpha E_0 \tag{2}$$

Since these parameters are applied at meso-scale, they are different from the elastic parameters describing overall behavior of material - Young's modulus $E$ and Poisson's ratio $\nu$. Their approximate relation derived in [9, 5, 7] results in equations

$$E_0 = \frac{E}{1-2\nu} \qquad \alpha = \frac{1-4\nu}{1+\nu} \tag{3}$$

Eq. (3) postulates limitation on Poisson's ratio, that must be within interval $(-1, 0.25)$. Nevertheless, value of Poisson's ratio for concrete is around $0.2$.

In nonlinear regime, isotropic damage model is applied. Damage at contacts is described by parameter $\omega \in \langle 0, 1\rangle$ - Eq. (1). The initially undamaged contact ($\omega = 0$) might, after reaching the strain at the elastic limit, gradually loose stiffness as the strain increases further. At $\omega = 1$, the contact is completely damaged and cannot transfer any stress again. The evolution of the damage parameter $\omega$ is a crucial part of the constitutive law. Its description is quite elaborative, interested reader is referred to [4, 6] for the detailed description.

Since the discretization of a material body comes from pseudo-random process, the response of simulations with different meso-scale geometry differs as well.

### 2.2 Dynamics

Fracture of concrete is a dynamic process. However for slow (so called quasi-static) loading rates, the solution can be obtained under assumption of static equilibrium. For higher strain rates, the influence of inertia cannot be neglected and time-dependent response should be calculated. It is usually obtained from solution of differential equations of motion

$$\boldsymbol{M}\ddot{\boldsymbol{u}} + \boldsymbol{C}\dot{\boldsymbol{u}} + \boldsymbol{K}\boldsymbol{u} = \boldsymbol{F} \tag{4}$$

where $\boldsymbol{M}$, $\boldsymbol{C}$ and $\boldsymbol{K}$ stand for mass, damping and stiffness matrix, $\boldsymbol{F}$ and $\boldsymbol{u}$ is loading and displacement vector, respectively. Dotted symbol of displacement vector denotes its derivative with respect to time, which is velocity (first derivative) and acceleration (second derivative).

Numerical algorithms for solving equations of motion are divided into explicit and implicit time integration schemes, depending on the time the equilibrium is considered at. In case of explicit algorithms, the solution for time $t + \Delta t$ is calculated from equilibrium at time $t$ directly by matrix and vector multiplication; there is no system of equations to solve. But the numerical solution is only conditionally stable, the time step length $\Delta t$ is restricted by the smallest natural frequency of the system, which often brings need for using large number of very short time steps. Therefore, the explicit algorithms are convenient for solving events with short duration, e.g. impact loading.

In an implicit time integration scheme, the solution at time $t + \Delta t$ is calculated from Eq. (4) assembled at time $t + \Delta t$. Its advantage is unconditional stability, the step length is controlled purely by accuracy. But to obtain such solution, system of dependent equations has to be solved.

These equations are nonlinear in the case of nonlinear material, so each time step involves an iterative process to find the solution. These algorithms are conveniently used for solution of processes with longer duration, e.g. structural response during earthquakes.

For the purpose of this contribution, Newmark implicit scheme [11] is implemented. Velocity ($\dot{\boldsymbol{u}}$) and accelerations ($\ddot{\boldsymbol{u}}$) are approximated by

$$\ddot{\boldsymbol{u}}_{t+\Delta t} = \frac{1}{\beta \Delta t^2} \left( \boldsymbol{u}_{t+\Delta t} - \boldsymbol{u}_t \right) - \frac{1}{\beta \Delta t} \dot{\boldsymbol{u}}_t - \left( \frac{1}{2\beta} - 1 \right) \ddot{\boldsymbol{u}}_t \tag{5}$$

$$\dot{\boldsymbol{u}}_{t+\Delta t} = \dot{\boldsymbol{u}}_t + \Delta t \left( 1 - \gamma \right) \ddot{\boldsymbol{u}}_t + \gamma \Delta t \ddot{\boldsymbol{u}}_{t+\Delta t} \tag{6}$$

where index $t$ refer to solution from previous time step. $\beta$ and $\gamma$ are Newmark parameters within interval $\langle 0, 1 \rangle$. To keep the solution unconditionally stable, they must satisfy condition $2\beta \geq \gamma \geq 0.5$ [1]. The only unknown in Eqs. (5) and (6) is vector of displacement at time $t + \Delta t$. To calculate the displacement in time $t + \Delta t$, the approximations are plugged into Eq. (4) and the following system is obtained

$$\left( \boldsymbol{K} + \frac{1}{\beta \Delta t^2} \boldsymbol{M} + \frac{\gamma}{\beta \Delta t} \boldsymbol{C} \right) \boldsymbol{u}_{t+\Delta t} = \boldsymbol{F}_{t+\Delta t} + \boldsymbol{M} \left( \frac{1}{\beta \Delta t^2} \boldsymbol{u}_t + \frac{1}{\beta \Delta t} \dot{\boldsymbol{u}}_t + \left( \frac{1}{2\beta} - 1 \right) \ddot{\boldsymbol{u}}_t \right) + \\ + \boldsymbol{C} \left( \frac{\gamma}{\beta \Delta t} \boldsymbol{u}_t + \left( \frac{\gamma}{\beta} - 1 \right) \dot{\boldsymbol{u}}_t + \frac{\Delta t}{2} \left( \frac{\gamma}{\beta} - 2 \right) \ddot{\boldsymbol{u}}_t \right) \tag{7}$$

where effective stiffness matrix multiplied with unknown displacement vector $\boldsymbol{u}_{t+\Delta t}$ stands on the left side and the effective loading vector on the right side of the equation. Note that the nonlinear material formulation brings dependence of the stiffness matrix on the displacements, so the solution is searched in an iterative Newton process.

Mass matrix $\boldsymbol{M}$ is not diagonal because the effect of rotational inertia. Shape of the particle is (due to Voronoi tessellation) convex polyhedron that can be decomposed into simplexes (tetrahedra). Tetrahedra inertia tensors are calculated from their vertex coordinates according to [14] and further combined using parallel axis theorem to obtain inertia tensor of a whole particle. Since the model assumes small deformations and rotations, calculation is geometrically linear and mass matrix is constant during the whole simulation. Damping is not considered within this contribution.

## 3 NUMERICAL SIMULATIONS

### 3.1 Geometry and material properties

The model described in the previous sections is applied to simulate set of concrete specimens loaded under various displacement rates. The experimental series of concrete specimens with a shape of an upside down letter L [12] is simulated. Specimen dimensions are $W, D = 500\,\text{mm}$ and $W_1, D_1 = 250\,\text{mm}$ (Fig. 1). Specimen thickness is $t = 50\,\text{mm}$. Depth of the bottom support is $100\,\text{mm}$ and loading is applied in a distance of $30\,\text{mm}$ from the edge of the specimen. Loading is applied by increasing deformation at constant velocity and the loading force is calculated during the simulations. Loading rates are chosen according to [12] as $0.25\,\text{mm/s}$ for quasi-static loading and 0.1, 0.35, 0.74, 1.0 and 2.4 m/s to study the influence of strain rate.

Material parameters are taken from [12]. Macroscopic Young's modulus is $E = 32.2\,\text{GPa}$ and Poisson's ratio is $\nu = 0.18$; the corresponding elastic meso-scopic parameters at the interparticle contacts are obtained from Eq. (3): meso-scale elastic modulus $E_0 = 50$ GPa and normal-tangential stiffness ratio $\alpha = 0.237$, respectively. Further material properties

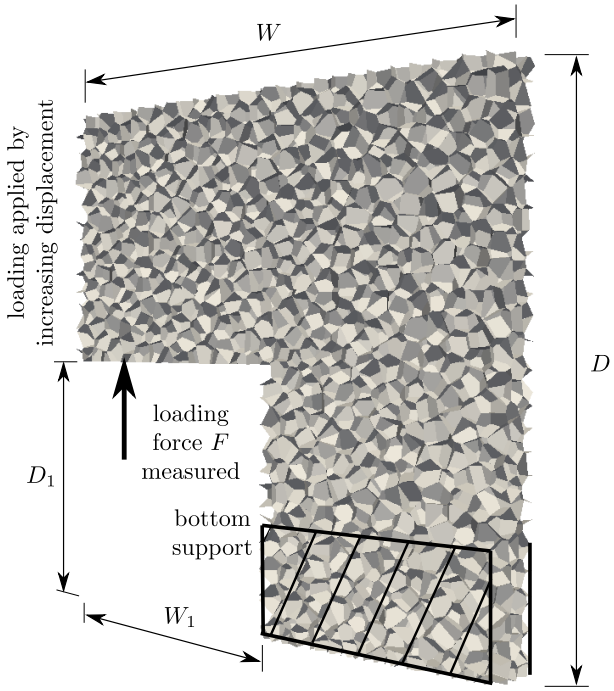


Figure 1: Geometry of simulated specimen showing particle model structure.

taken from [12] are the following: material density $\rho = 2210\,\mathrm{kg/m^3}$ and tensile strength $f_t = 3.12\,\mathrm{MPa}$. The meso-scopic fracture energy for tensile failure was identified from the quasi-static loading rate according to the experiments as $G_f = 35.5\,\mathrm{N/m^2}$. Other properties defining the constitutive relations of the model are obtained from the listed parameters according to the recommendations in [4].

### 3.2 Influence of material parameters

For static loading, both the elastic and fracture material characteristics plays a crucial role. The maximum loading force is mainly influenced by the stiffness parameter $E_0$, tensile strength $f_t$ and meso-scopic fracture energy $G_f$. There is no effect of material density, $\rho$. With increasing loading rate, the effect of fracture parameters diminish, the most important material parameters become $E_0$ and $\rho$.

To demonstrate this trend, influence of these material properties was studied. The structural response was calculated with 1.5 $\times$ increased parameters $E_0$, $f_t$, $G_f$ and $\rho$. Model response is plotted in graphs in Fig. 2. The percentual change of maximum load for increased values of parameters is shown in Fig. 3. The elastic modulus $E_0$ is strongly influential for all displacement rates. The influence of tensile strength $f_t$ and fracture energy $G_f$ at increased loading rate almost disappear, while the influence of material density $\rho$ takes their place. However, the influence of the fracture parameters appears again for rates larger or equal to 0.74 m/s. This is caused by cracking in the area of applied load (Fig. 5), which was not observed experimentally in [12].

To demonstrate that the cracking at loading is responsible for re-appearance of the fracture parameters among the influential material parameters for high displacement rates, the model made of ideally elastic material was analyzed. In Fig. 4, experimental, elastic and inelastic responses are shown. One can see that for rate 0.1 m/s, the elastic and inelastic models behave

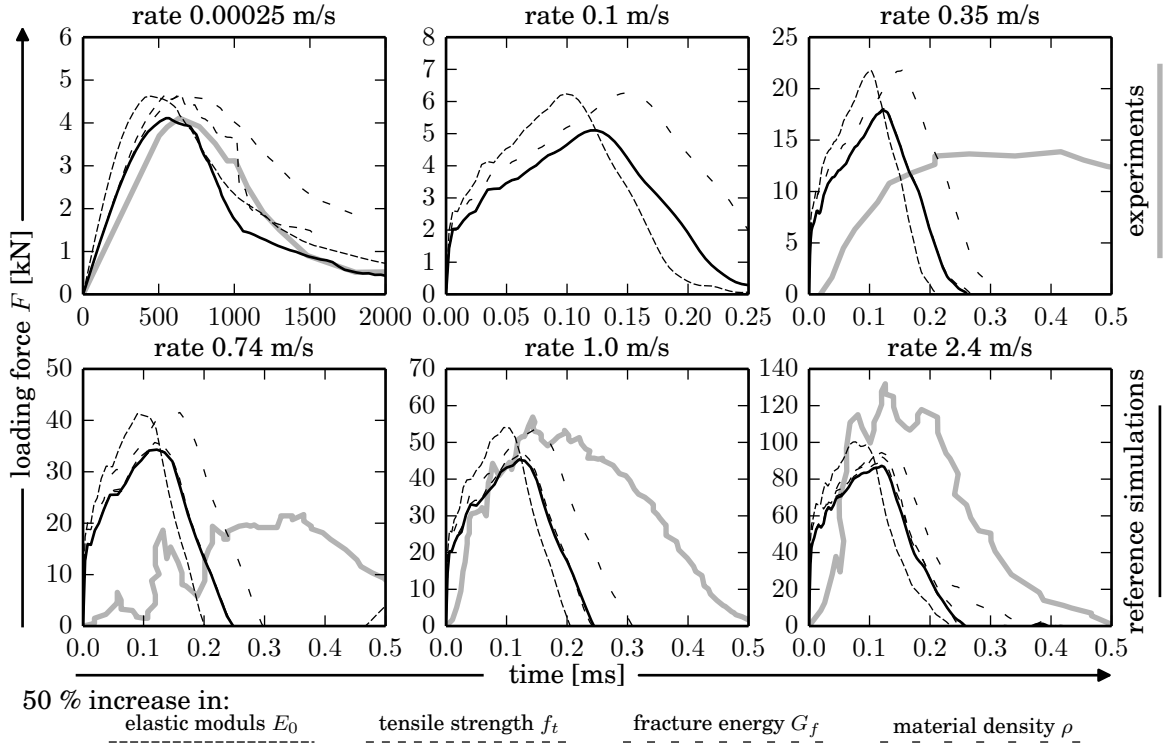


Figure 2: Response of numerical simulations at various displacement rates compared with experimental curves from [12].

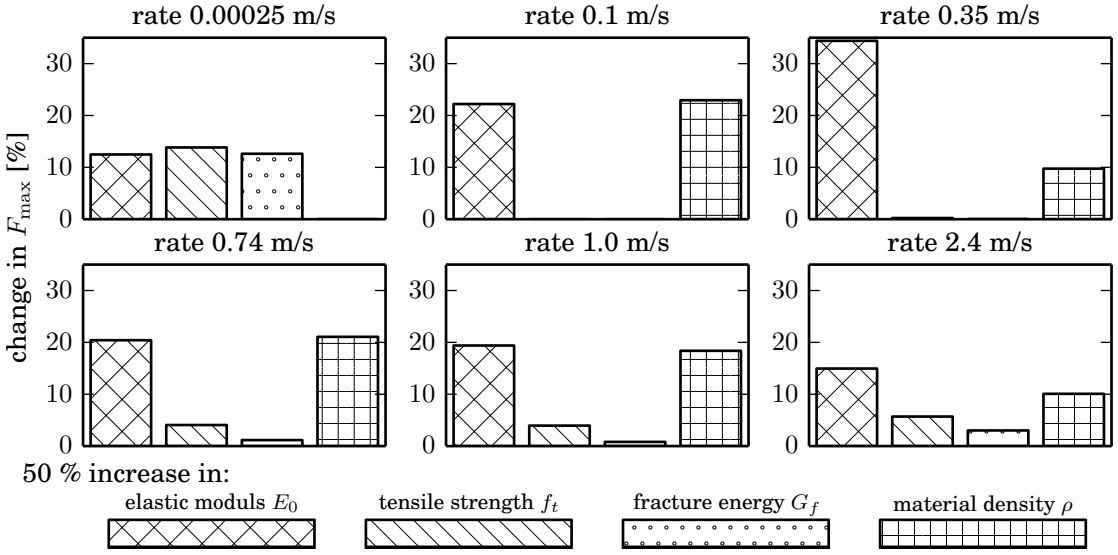


Figure 3: Effect of selected material parameters at various displacement rates.

the same. The cracking does not have any effect on loading force. But for rates 1.0 m/s and 2.4 m/s, the cracking effect appears. Therefore, the inelastic processes must happen much closer to the loading point, i.e. in the loading area.

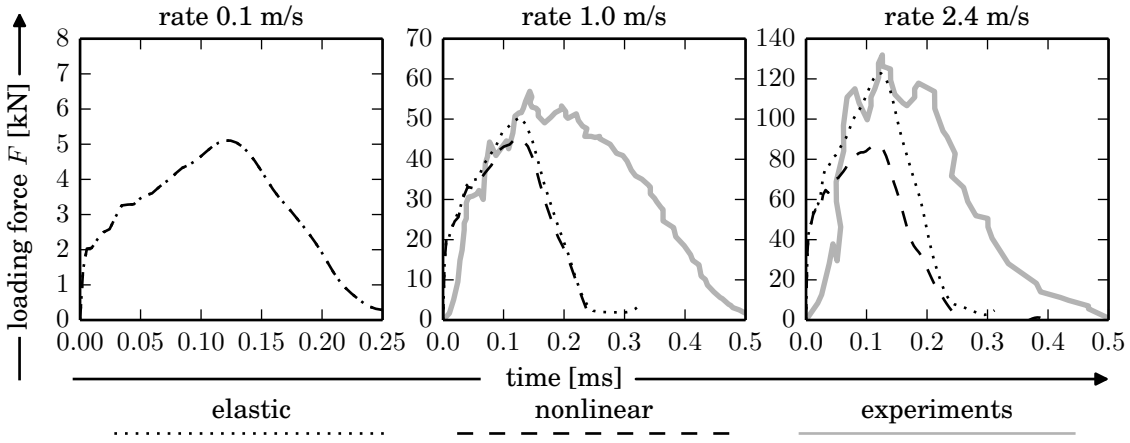


Figure 4: Comparison of nonlinear vs. elastic response of the model

### 3.3 Crack patterns

In Fig. 5, the discrete structure representing material is plotted. Facets (contacts between particles) are colored according to their damage parameter $\omega$ at the end of the simulation. These damaged facets represent crack in the material. One can see different crack path for different loading rates, the trend is in agreement with the experiment [12]. For quasi-static loading, the crack propagates in horizontal direction. With increasing loading rate, crack changes its direction towards vertical. When the velocity of applied load is increased further, multiple cracking and crack branching occur. The experimental evidence, however, does not show extensive cracking in the loading area at rate 2.4 m/s.

### 3.4 Peak loads

The agreement of the model response and experimental data is rather poor. Reasonable match is for quasi-static rate, where the material parameters were identified. For rates 0.35 and 0.74 m/s, the model overestimates the maximum loads, while for rate 1.0 and 2.4 m/s, the experimental response yields higher peak loads. This can be seen in Fig. 6, where experimental and simulated elastic and inelastic maximum forces are plotted. When talking about peak force in elastic simulation, we mean the first peak in the response. Of course, response of all elastic simulations oscillates around the static solution which is increasing to infinity. There is no peak in quasi-static solution so that data-point is missing in Fig. 6.

The elastic responses for the two highest loading rates agree with the experiment very well. If one can eliminate cracking from the loading area, the agreement between the model and experiment would be reasonable. The other two intermediate rate already behaves as if the model is elastic, no improvement can be expected there. However, looking at Fig. 6, these two intermediate rate shows unexpectedly low experimental peak forces compared to the higher rates. Therefore, we consider the difference to be related to the inevitable experimental scatter.

One way how to eliminate the cracking in the loading area for high loading rates can be gradual increase in displacement rate $v$. Instead of direct application of the loading velocity, we intruduced smooth transition controlled by single parameter $t_0$.

$$u_l = \begin{cases} \left(0.5t^2 + \frac{t_0}{4\pi^2}\cos(2\pi\frac{t}{t_0}) - \frac{v}{t_0}\right)\frac{v}{t_0} & t \le t_0 \\ v\ t - v\ t_0\ u_l(t_0) & t > t_0 \end{cases} \tag{8}$$

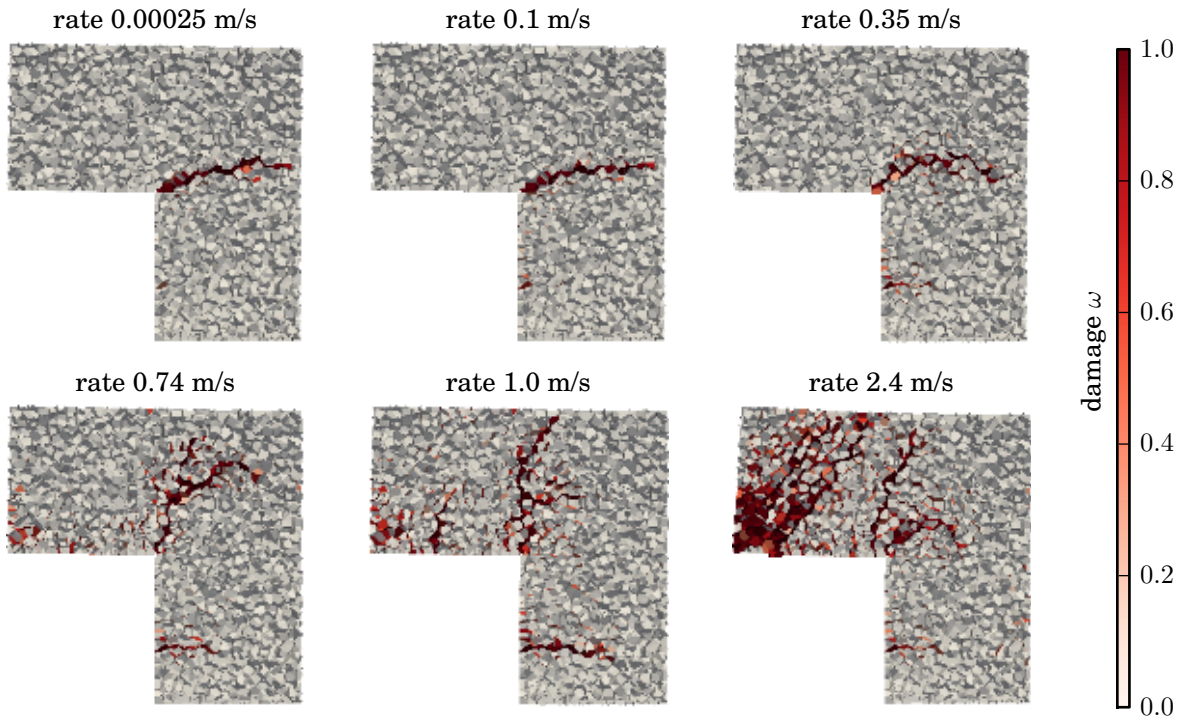


Figure 5: Different crack pattern obtained with particle model for various displacement rates.

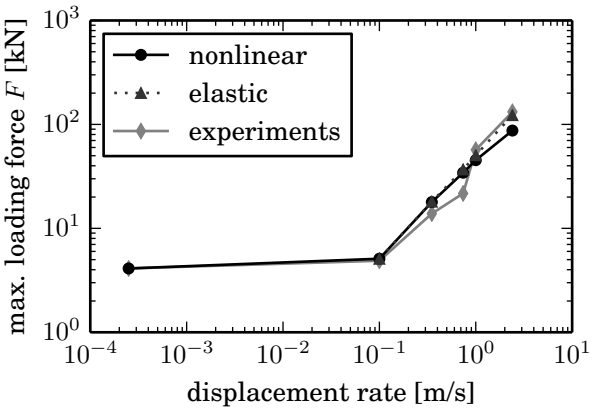


Figure 6: Relation between maximum loading force and displacement rate.

where $u_l$ is the applied displacement at the area of loading and $t_0$ is initial transition period after which correct loading velocity is achieved. This analytical formula ensures smooth transition from initial motionless state to full loading speed for displacements, velocities and accelerations.

Using formula (8), simulations of specimens loaded under displacement rate 2.4 m/s were performed. Obtained responses and cracks pattern are shown in upper part of Fig. 7. Some reduction of crushing close to the loading point is possible. However to eliminate it or at least substantially reduce, time $t_0$ needs to be relatively large, the maximum force occurs in the transitional time and the full displacement rate is achieved too late.

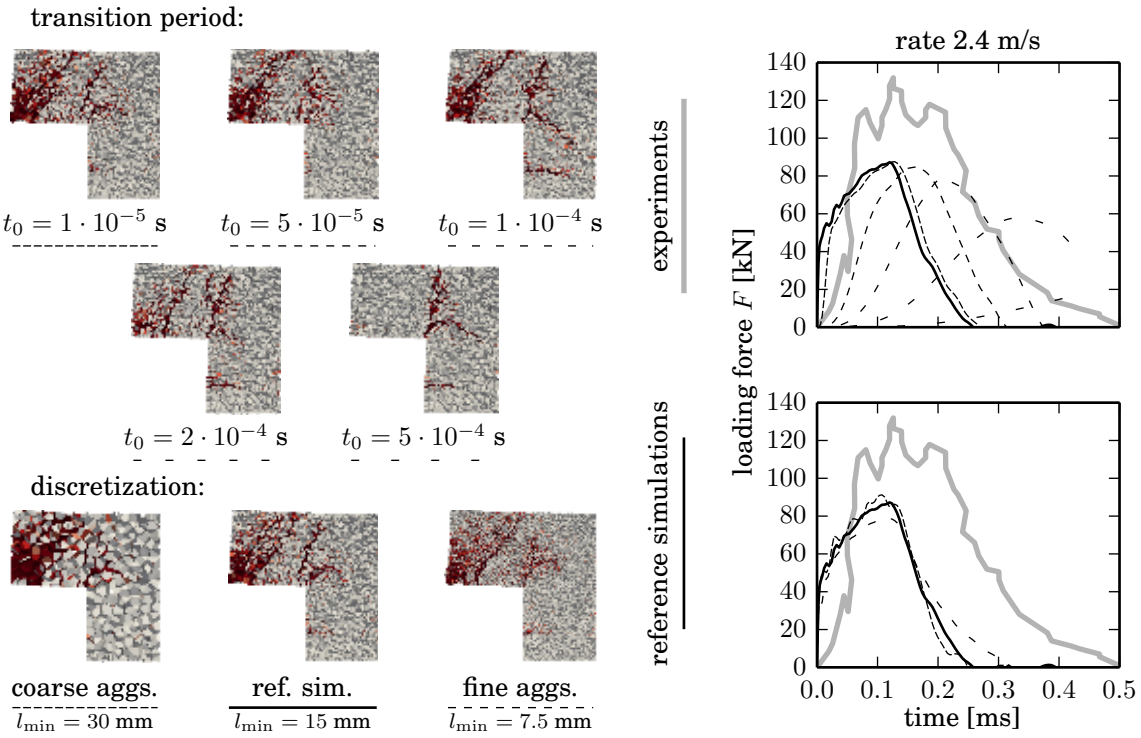


Figure 7: Effect of gradual increase of displacement rate and particle size.

Up to this point, particle size $l_{\min} = 15$ mm was used. Since this model uses crack band concept [3], the discretization does not influences the model response for cases where the crack is localized. However, the cracking in the loading area is highly distributed and strong dependence on discretization density is expected. The results for simulation using doubled and halved particle size are shown in lower part of Fig. 7. Note that for coarse discretization there are only two particles within the specimen thickness. The finer (coarser) discretization yields lower (higher) peak loads than the reference simulation, respectively. This increase or decrease in the peak load can be at least partially caused by the random discretization of the model geometry as mentioned in sec. 2.1.

## 4 CONCLUSIONS

The presented discrete model was used for dynamic simulations of concrete specimens loaded under various displacement rates. The influence of material properties on the time dependent response was studied. The major trend is that the higher loading rates lead to increased effect of density and reduced effect of nonlinear material properties. However, local cracking in the loading area brings back the influence of nonlinear material parameters for very high loading rates.

Expected increase in the maximum loading force and change in the mechanism of failure with increasing strain rate was observed. Comparison to the experimental data [12] shows discrepancies. These differences are caused by cracking in the loading area, which was not observed in the experiment.

## 5 ACKNOWLEDGEMENTS

Financial support provided by the Czech Science Foundation under project No. 15-19865Y and additional support by project No. FAST-J-17-4583 is gratefully acknowledged.

## REFERENCES

[1] K.-J. Bathe. *Finite element procedures*. Prentice Hall, Englewood Cliffs, N.J., 1996.

[2] Z. P. Bažant and F.B. Lin. Nonlocal smeared cracking model for concrete fracture. *Journal of Structural Engineering*, 114(11):2493–2510, 1988.

[3] Z.P. Bažant and B.H. Oh. Crack band theory for fracture of concrete. *Matriaux et Constructions*, 16(3):155–177, 1983.

[4] G. Cusatis and L. Cedolin. Two-scale study of concrete fracturing behavior. *Engineering Fracture Mechanics*, 74(1-2):3–17, 2007.

[5] Gianluca Cusatis, Daniele Pelessone, and Andrea Mencarelli. Lattice discrete particle model (LDPM) for failure behavior of concrete. I: Theory. *Cement & Concrete Composites*, 33(9):881–890, 2011.

[6] J. Eliáš. Adaptive technique for discrete models of fracture. *International Journal of Solids and Structures*, 100–101:376–387, 2016.

[7] J. Eliáš. Boundary layer effect on behavior of discrete models. *Materials*, 10(2):157, 2017.

[8] Y.K. Hwang, J.E. Bolander, and Y.M. Lim. Simulation of concrete tensile failure under high loading rates using three-dimensional irregular lattice models. *Mechanics of Materials*, 101:136–146, 2016.

[9] E. Kuhl, G.A. D'Addetta, H.J. Herrmann, and E. Ramm. A comparison of discrete granular material models with continuous microplane formulations. *Granular Matter*, 2(3):113–121, 2000.

[10] J. M. Melenk and I. Babuška. The partition of unity finite element method. *Computer Methods in Applied Mechanics and Engineering*, 139:289–314, 1996.

[11] N. Newmark. *A method of computation for structural dynamics*. University of Illinois, Urbana, 1959.

[12] J. Ožbolt, N. Bede, A. Sharma, and U. Mayer. Dynamic fracture of concrete l-specimen. *Engineering Fracture Mechanics*, vol. 148:27–41, 2015.

[13] J. Smith and G. Cusatis. Numerical analysis of projectile penetration and perforation of plain and fiber reinforced concrete slabs. *International Journal for Numerical and Analytical Methods in Geomechanics*, 41(3):315–337, 2017.

[14] F. Tonon. Explicit exact formulas for the 3-D tetrahedron inertia tensor in terms of its vertex coordinates. *Journal of Mathematics and Statistics*, 1(1):8–11, 2005-1-1.

[15] J. G. M. van Mier. *Concrete fracture*. CRC Press, Boca Raton, FL, 2013.